PERGAMON

International Journal of Heat and Mass Transfer 46 (2003) 879–888

International Journal of HEAT and MASS TRANSFER

www.elsevier.com/locate/ijhmt

Real-time laser-based measurement of interface temperature during droplet impingement on a cold surface

Q. Chen, Y. Li, J.P. Longtin *

Department of Mechanical Engineering, State University of New York at Stony Brook, Stony Brook, NY 11794–2300, USA

Received 1 October 2001; received in revised form 13 June 2002

Abstract

This work presents a laser-based thermoreflectance technique to measure the real-time change in temperature of a liquid–solid interface when a heated liquid droplet impinges on a transparent substrate. Temperature variation at the interface results in refractive index changes in both the liquid and substrate, which, in turn, cause a reflectivity change at the interface. A 5 mW HeNe laser and a silicon photodiode are used to monitor the real-time reflectivity of the interface. The measurement is performed with two liquids, water and glycerol, impinging onto one surface of a prism made of F2 glass, with initial liquid temperatures of 0, 25, and 45 °C above room temperature. A temporal resolution of 8.8 ms and spatial resolution of 180 μm have been achieved in this work. The measurement uncertainty is ~3.5–6.3 °C for water and 0.5 °C for glycerol. Higher temporal and spatial resolution can be readily obtained with minor modifications to the experimental apparatus. Measurement of liquid solidification and evaporation on a substrate may also be suitable for this technique, as the phase change causes an abrupt variation in reflectivity at the interface.

1. Introduction

Liquid droplets impinging upon a solid surface are present in a variety of important engineering and scientific applications. Examples include impingement cooling of surfaces, condensation phenomena in which liquid droplets fall and strike a surface, vigorous mixing of gas–liquid systems, and manufacturing, e.g., metal forming and coating processes. The liquid–solid interface temperature during droplet impinging on a solid surface plays a critical role in these applications; however, measuring the transient liquid–solid interface temperature remains an elusive and difficult task, especially for rapid temperature changes and small droplet size.

The fluid flow associated with impinging droplets is complicated [1]. The fluid dynamics of droplet impingement has been studied both theoretically and experimentally by many researchers [2–5]. Hatta et al. [6] investigated the collision dynamics of a water droplet impinging on a rigid surface at room temperature. They simulated the deformation behavior and flow field inside the droplet numerically, and it was found that the liquid film formed by the impinging droplet on the surface spread radially along the solid surface and then began to recoil from the peripheral region towards the center after the radius reached a maximum. Shi et al. [7] measured the transient solid surface temperature using a surface temperature probe. While this method is of considerable merit, it has certain limitations; for example, the intrusive nature of the gap in the aluminized surface used for temperature sensing affects the spread and the recoil dynamics, especially for small droplets. Also the surface temperature probe can only measure the temperature within the solid substrate, rather than the actual liquid–solid interface temperature. Cokmez-Tuzla et al. [8] applied a microthermocouple to study liquid-wall convective boiling. In their work, the sensing tip of the thermocouple was 15–18 μm in diameter, and temperature was measured roughly 16 μm beneath the solid surface. Although many efforts have been made to study

* Corresponding author. Tel.: +1-631-632-9436; fax: +1-631-632-8544.

E-mail address: jlongtin@ms.cc.sunysb.edu (J.P. Longtin).

0017-9310/03/$ - see front matter
PII: S0017-9310(02)00298-3

Nomenclature

b	effusivity (J/K m^2 s$^{1/2}$)
C_p	specific heat (J/kg K)
I	laser intensity (W)
k	thermal conductivity (W/m K)
n	refractive index
R	reflectivity
t	time (s)
T	temperature (K or °C)
V	voltage (V)
x	direction normal to interface (m)
Greek symbols	
α	angle of incidence at air–glass interface (°)
α_T	thermal diffusivity (m^2/s)
β_i	angle of incidence in glass (°)
β_r	angle of refraction in glass (°)
γ	angle of refraction in liquid (°)
λ	laser wavelength (m)
θ	angle of incidence and refraction (°)
ρ	density (kg/m^3)
Subscripts	
0	initial, reference
1, 2	medium 1, medium 2; interface 1, interface 2
3	final
a	air
g	glass
int	interface
l	liquid
p	p-polarized light
s	s-polarized light

the fluid and thermal characteristics of droplet impingement, to the authors' knowledge, the true interface temperature during droplet impinging on a solid surface has not yet been accurately measured. In particular, techniques that require physical contact with the fluid can disturb the flow and heat transfer, and also cannot obtain the true interface temperature.

Due to their unique features, laser-based measurement techniques have played a significant role in scientific and engineering investigations. These techniques have the advantages of non-invasiveness, remote sensing, and high spatial and temporal resolutions. Qiu et al. [9] applied a thermoreflectance technique to measure the temperature of solid silicon. Lee and Norris [10] used a polarization-differential reflectance method to monitor small temperature variations in a thin solid film with a temporal resolution of 10 ms. A laser-based technique to measure the time-dependant solid–liquid interface temperature with a relatively long time scale (~10 min) was recently presented by Fan and Longtin [11], in which the temperature of several flowing bulk liquids at a transparent solid–liquid interface was measured and compared with a calibrated thermistor, with good agreement found.

Several laser-based techniques have been applied to investigate droplet impingement phenomena. Müller et al. [12] measured the temperature of liquid methanol and ethanol in an atomized spray using a thermometry method to obtain the droplet temperature. Zhao and Poulikakos [13] used a laser-based photoelectric technique to measure the transient splat radius for both molten solder and water droplets impinging on a quartz plate. This work presents a laser-based thermoreflectance technique to measure the liquid–solid interface temperature for a liquid droplet impinging on a transparent solid surface provided by an equilateral optical prism. The thickness of the interrogated region at the interface is on the order of $\lambda/2$ [14], where $\lambda = 632.8$ nm is the incident laser wavelength, giving a very good estimate of the actual interface temperature.

In this experiment, the temporal resolution of the experiment is roughly 8.8 ms, and the spatial resolution is ~180 μm. The temporal resolution of the measurement is limited by the electrical components, rather than the optical components, while the beam spot size determines the spatial extent of the measurement region, and can be reduced to ~20 μm or less at the solid–liquid interface using a focusing lens. Thus higher temporal spatial resolution can be readily obtained with minor modification.

2. Experimental setup

The experimental configuration is shown in Fig. 1. A beaker containing test liquid and a magnetic stirring bar is placed on a hot plate, where the test liquid is circulated, mixed, and uniformly heated. The liquid temperature is measured by a reference thermocouple immersed in the liquid, which has been calibrated against a NIST-traceable RTD probe over the temperature range 15–80 °C. When the test liquid is heated to the desired temperature, a micropipettor is used to dispense a known volume of liquid above the solid surface. The micropipettor is then placed in a holder to control the droplet impingement height and angle. The droplet impinges on one surface of an equilateral optical prism made of F2 glass with an edge length of 30 mm that is mounted such that the im-

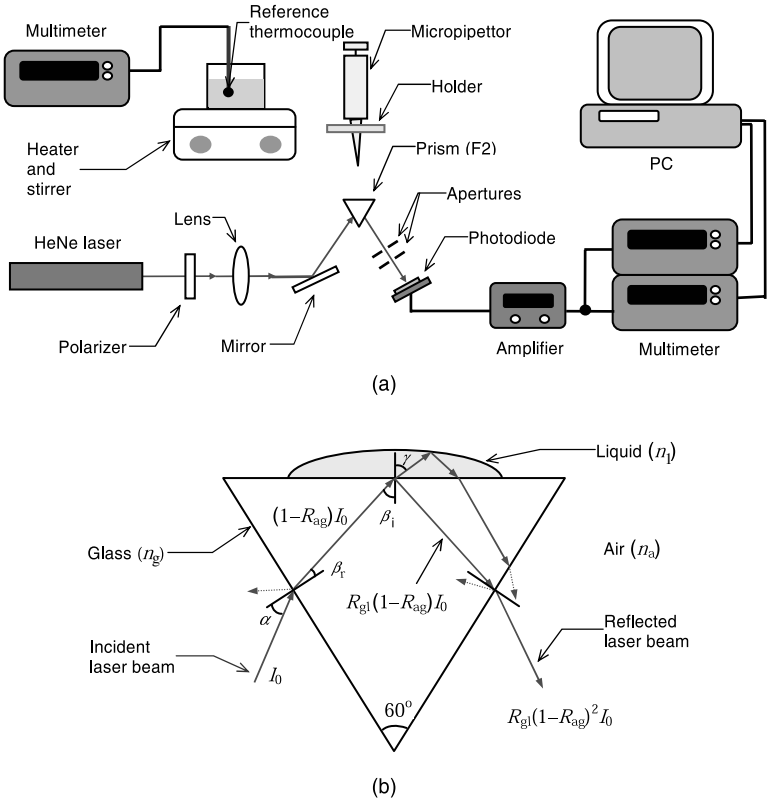

Fig. 1. (a) Experimental setup and (b) details of beam propagation and reflection.

pinging surface is horizontal. The prism provides high transmittance through the visible spectrum and a smooth, flat surface for the liquid–solid interface.

A 5 mW HeNe laser with a wavelength of 632.8 nm serves as the light source. The laser beam is linearly polarized using a Newport Glan-Thompson calcite polarizer. To obtain a smaller beam spot size for higher spatial resolution, a lens with a focal length of 100 mm is used to focus the beam. After focusing, the beam strikes a mirror mounted on a rotational stage that directs the beam to one side of the equilateral optical prism adjacent to the horizontal impinging surface at the desired angle of incidence (Fig. 1).

The reflected beam from the liquid–glass interface, which exits from the other side of the prism (Fig. 1b), is sent to a UDT PIN-6D silicon PIN photodiode (PD) with an active area of 20.3 mm^2. The PD current is then sent to a Melles Griot 13AMP005 transimpedance (current-to-voltage) amplifier and converted to a voltage that is linearly proportional to the photodiode current. Since only the reflected beam from the liquid–solid interface is of interest, two collinear apertures are used to keep other beams (e.g., reflected beam from the liquid–air interface in Fig. 1b) from striking the photodiode. Two Keithley Model 2000 voltmeters operated at different sampling rates are applied to monitor the voltage change from the amplifier to provide both high-resolution and long-term data acquisition. The readings from the voltmeters are sent to a personal computer via a GPIB interface for data acquisition. The first voltmeter stores readings internally in the buffer at a sampling rate of 114 samples/s. Since the buffer holds only 1024 readings, only about 9.0 s of data can be taken using this voltmeter. The second meter has a sampling rate of 5 samples/s and a very large buffer, and allows the measurement of the interface temperature until it reaches room temperature.

To minimize noise, the experiment is assembled on a vibration-isolated optical bench. Care was taken to adjust the angle of incidence accurately during setup. First, the laser beam is aligned horizontally to the bench, and then the polarizer and optical lens are inserted and aligned such that the beam propagation does not deviate from the original direction. Next, the mirror was mounted so that the incident and the reflected beams overlap, corresponding to normal incidence. The reading on the rotational stage is then recorded as a reference. Finally, the stage, on which the mirror is mounted, is rotated to obtain the desired angle of the incidence on the prism surface (Fig. 1).

3. Theory

The experiment principle is based on the thermoreflectance, i.e., the variation in intensity of reflected light from the liquid–solid interface as a function of temperature. The reflectivity of the interface is determined by the refractive indices of both the liquid and solid, which, in turn, depend on the temperature; therefore, by measuring the change in intensity of light reflected from the interface, the temperature at the interface can be obtained.

If I_0 is the intensity of the incident laser beam on the interface and R the reflectivity of the interface, the intensity of the reflected beam will be RI_0. From Fresnel's law of reflection [15], R depends on the angle of incidence and the beam polarization:

$$R_s = \left[\frac{\sin(\theta_1 - \theta_2)}{\sin(\theta_1 + \theta_2)}\right]^2 \tag{1}$$

$$R_p = \left[\frac{\tan(\theta_1 - \theta_2)}{\tan(\theta_1 + \theta_2)}\right]^2 \tag{2}$$

where R_s is the reflectivity of s-polarized light, R_p the reflectivity of p-polarized light, and θ_1 and θ_2 are the angles of incidence and refraction, respectively.

In this experiment, there are three interfaces involved: the two air–glass interfaces on the lower positions of the prism, and the glass–liquid interface at the top (Fig. 1b). According to Snell's law of refraction in Fig. 1b:

$$n_a \sin\alpha = n_g \sin\beta_r \tag{3a}$$

$$n_g \sin\beta_i = n_l \sin\gamma \tag{3b}$$

$$\beta_r + \beta_i = \frac{\pi}{3} \tag{3c}$$

where α and β_i are the angles of incidence at which the laser beam strikes the side surface of the prism and the glass–liquid interface, β_r and γ are the angles of refraction in the prism and liquid, and n_a, n_g, and n_l are the refractive indices of air, glass, and liquid, all respectively.

Angles β_r and β_i are related by Eq. (3c) for an equilateral prism as shown in Fig. 1b, and, in turn, both depend on the incident angle α and the glass refractive index. Therefore, from Eqs. (1), (2), (3a)–(3c), it is seen that the reflectivity of the liquid–solid interface is determined by the incident angle α, and the refractive indices of glass n_g and liquid n_l:

$$R_s = R_s(\alpha, n_g, n_l) \tag{4}$$

$$R_p = R_p(\alpha, n_g, n_l) \tag{5}$$

For both the prism and pure liquid, the refractive index depends on the wavelength and the temperature: $n = n(\lambda, T)$, neglecting strong pressure variations. Since the HeNe laser is highly monochromatic ($\lambda = 632.8$ nm), the wavelength variation can be neglected. Hence, for a fixed angle of incidence, the reflectivity depends only on the interface temperature. For both s- and p-polarized light the change in reflectivity with the temperature can be expressed as:

$$\Delta R \cong \left[\frac{\partial R}{\partial n_g}\frac{dn_g}{dT} + \frac{\partial R}{\partial n_l}\frac{dn_l}{dT}\right]\Delta T \tag{6}$$

where ΔT is a finite temperature change at the interface, and ΔR represents the corresponding reflectivity change associated with temperature change ΔT. According to Eq. (6), the change in reflectivity is determined by the temperature coefficient dn/dT, the sensitivity of reflectivity to refractive index $\partial R/\partial n$, and interface temperature change ΔT.

The present technique measures the change in the reflectivity at the interface where the liquid and solid are assumed to be in perfect contact to obtain the temperature change at the interface. During the experiment, a liquid droplet with a given temperature is dropped onto the horizontal surface of the prism and allowed to reach thermal equilibrium at room temperature T_0, which corresponds to a reference reflectivity, R_0 and a voltage output V_0 from photodiode/amplifier. Due to the linear response of the photodiode and amplifier, the reflectivity change ΔR and voltage change ΔV can be related as follows:

$$\frac{\Delta R}{R_0} = \frac{\Delta V}{V_0} \tag{7}$$

Combining Eqs. (6) and (7), the temperature change can be expressed as:

$$\Delta T = \left[\frac{\partial R}{\partial n_g}\frac{dn_g}{dT} + \frac{\partial R}{\partial n_l}\frac{dn_l}{dT}\right]^{-1} R_0 \frac{\Delta V}{V_0} \tag{8}$$

To obtain a large signal-to-noise ratio, both a large sensitivity, i.e., $\Delta R/R_0$ for $\Delta T = 1$ K, and a reasonable overall reflectivity are desired. The sensitivity is determined by the polarization, the angle of incidence, and the refractive indices of liquids and glass through Eqs. (1), (2), (3a)–(3c). Using water on a prism made of F2 glass as an example, the reflectivity sensitivity of s-polarized light is shown in Fig. 2a, and is observed to decreases monotonically for $\alpha > 8°$ with the incident angle. For $\alpha < 8°$, the angle of β_i exceeds the critical angle and total internal reflection occurs at the water–glass interface. The sensitivity of p-polarized light behaves similarly, though it is larger for $\alpha \lesssim 25°$ and approaches infinity at $\alpha \approx 34°$, which corresponds to the Brewster angle (β_i) at the liquid–solid interface. Following the laser beam through the prism, the final intensity of the reflected light striking the photodiode is:

$$I_3 = I_0(1 - R_{ag})^2 R_{gl} \tag{9}$$

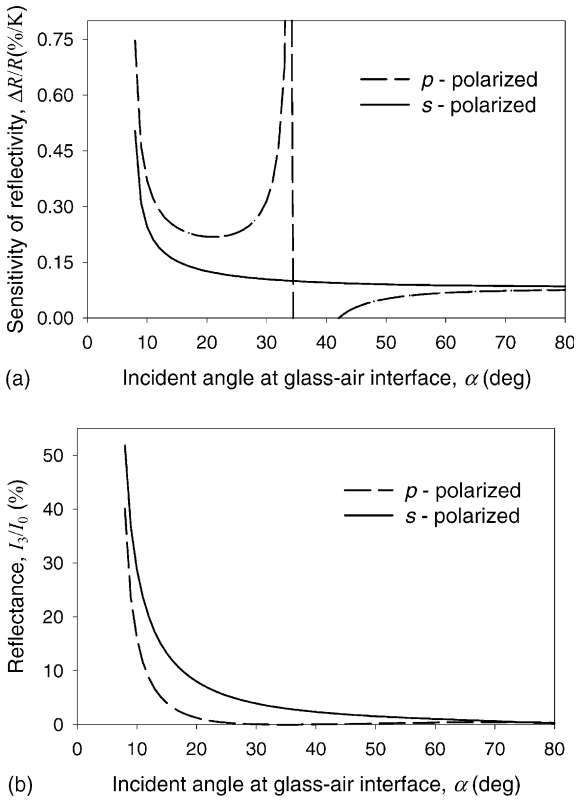

Fig. 2. (a) Sensitivity and (b) reflectivity for p- and s-polarized light versus incidence angle for water on an F2 prism.

where I_0 is the initial incidence intensity of the laser beam, I_3 is the laser intensity exiting the prism and striking the photodiode, and R_{ag} and R_{gl} are the reflectivities of the air–glass and glass–liquid interfaces, respectively (Fig. 1b). The intensity change of both s-polarized light and p-polarized light with the angle of incidence for water on the F2 prism at $\Delta T = 0$ °C is shown in Fig. 2b. For glycerol, the changes of sensitivity and intensity with incident angle are similar to those of water except that total internal reflection will not occur, even for $\alpha = 0°$ due to the small difference between refractive indices of glycerol and the F2 prism (Table 1). In this work, to provide maximum sensitivity and a large reflected intensity, s-polarized light with an incidence angle of 8° for water and 0° for glycerol is used.

4. Results and discussion

4.1. Results analysis

In this work, pure water and glycerol are used to demonstrate the transient interface temperature measurement technique with an equilateral optical prism as the solid substrate. All materials were chosen due to their well-documented thermal and optical properties, which are listed in Table 1. Values of the refractive index, n, and its temperature coefficient, dn/dT, are taken directly from the literature. Values of dn/dT for water are averaged from several sources [16,17], as reported values can vary by up to 14%. The value of dn/dT for F2 glass [18] is 0.036×10^{-4} K^{-1}, and is over 25 times smaller than dn/dT for water and glycerol [19,20]. Though refractive index changes due to temperature variations in the glass are retained in this analysis, their contribution is small compared with that from the test liquid.

In theory, the thickness of the liquid–solid interface is assumed to be infinitesimal; however, the actual interrogated region at the interface is a finite value on the order of one half the laser wavelength, $\lambda/2$ [14]. The laser source used has a wavelength of 632.8 nm; hence the effective thickness of the liquid region whose temperature is measured is on the order of 300 nm, which is a very good approximation to the true interface temperature. Even the smallest commercially available thermocouple, in contrast, is several hundred microns in diameter.

The temporal resolution for this technique is limited only by the electronics in the system, including the photodiode and amplifier response time, and the data acquisition-sampling rate. The PD and amplifier response time is on the order of 1 μs or less, while the

Table 1
Optical and thermal properties of water, glycerol, and F2

	n ($\lambda = 632.8$ nm)	dn/dT ($\times 10^{-4}$ K^{-1})	k (W/m K)	ρ (kg/m^3)	C_p (J/kg K)	α_T ($\times 10^{-6}$ m^2/s)
Water	1.331[a]	−0.8[a] −1.04[c]	0.607[b]	996.9[b]	4180[b]	0.146[b]
Glycerol	1.4735[b]	−2.3[d]	0.292[b]	1256.7[b]	2380[b]	0.0976[b]
F2	1.617[e]	0.036[e]	0.780[e]	3610[e]	557[e]	0.388[e]

[a] Ref. [16].
[b] Ref. [19].
[c] Ref. [17].
[d] Ref. [20].
[e] Ref. [18].

maximum sampling rate of the data acquisition system is 114 Hz, corresponding to a temporal resolution of 8.8 ms, and represents the limiting factor in the acquisition time. Higher temporal resolution can be achieved with a faster data acquisition system. Sampling rates in excess of 1 MHz (1 μs resolution) should be possible with no alteration to the setup, though the time scale of the HeNe laser intensity fluctuations should be characterized at higher sampling rates.

The spatial resolution of the technique is limited by the spot size of the laser beam at the interface. The spatial profile of the HeNe laser beam is Gaussian, and has a diameter of 0.85 mm at the laser exit. A quartz lens with focal length $f = 100$ mm is used to reduce the beam spot size at the interface. The beam diameter at the lens focal point was measured using a knife-edge technique and found to be 100 μm, while the calculated Raleigh range for this beam/lens system is ~7 mm [21]. The beam spot size at the liquid–glass interface elongates due to the high incident angle β_i (55°–60°), resulting in an elliptical spot size roughly 90 μm × 180 μm.

The volume of liquid dispensed from the micropipettor is 40 μl, with this volume chosen to provide a small droplet with adequate coverage of the beam spot when dropped. The nominal fall distance of the droplet is 1 cm, which was kept consistent by placing the micropipettor in a mounted holder. To minimize the temperature drop of the liquid in the pipettor once removed from the liquid container, the micropipettor tip is stored in the heated liquid reservoir for a minimum of 10 min before starting the experiment, and the time between removing the micropipettor from the liquid bath and dispensing the drop is less than 5 s. Three cases have been conducted for both water and glycerol: $\Delta T_0 = 0$, 25, and 45 °C, where ΔT_0 is the initial temperature difference between the liquid and substrate at room temperature. The $\Delta T_0 = 0$ °C test is performed to validate the measurement and assess system noise, as there is almost no temperature change during this measurement.

The time of impact can be accurately determined from the reflectivity signal, which decreases dramatically when the droplet contacts the prism. The reason is that the difference Δn_{al} between the refractive indices of air and liquid is much greater than the refractive index change Δn of liquid as it cools after impinging on the window, e.g., for water, $\Delta n_{al} = 0.33$, while $\Delta n \approx 0.0045$ for $\Delta T_0 = 45$ °C. The curve in Fig. 3a depicts the detector voltage as the water droplet strikes the interface for $\Delta T_0 = 45$ °C. The large reflectivity at time $t = 0$ results from the air–glass interface; near $t = 2$ s, the droplet strikes the surface, and the reflectivity drops significantly because the refractive index of water is much closer to that of F2 ($n = 1.617$). On this scale, it is impossible to accurately monitor the cooling curve of the droplet, and the vertical scale must be expanded to observe the time-dependent interface temperature.

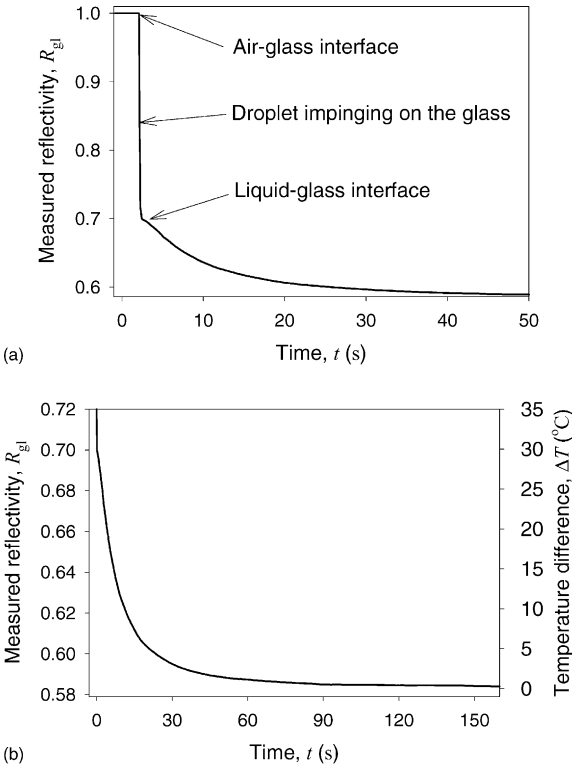

Fig. 3. (a) Measured signal—full scale and (b) measured signal and corresponding interface temperature difference for water at $\Delta T_0 = 45$ °C.

The detector voltage change and the corresponding temperature change from Eq. (8) for water at $\Delta T_0 = 45$ °C are shown in Fig. 3b for a period of 160 s. The time scale is adjusted such that $t = 0$ corresponds to droplet impingement. The rapid temperature change, which happens at the beginning of the droplet impinging on the substrate, cannot be accurately captured using the slow sampling rate meter, hence the data for the first eight seconds are taken from the faster buffered meter and the balance of the readings are from the slow meter. As can be seen, the temperature drops rapidly in the first 40 s, and then asymptotically approaches zero as t approaches 120 s.

The interface temperature measurements for water from the buffered meter for $\Delta T_0 = 0$, 25, and 45 °C are shown in Fig. 4. Note that a general feature of the measurement technique is a smooth, low-noise signal. The data are presented as collected from the meter: no smoothing or averaging is performed, and the results are repeatable. The case for $\Delta T_0 = 0$ is shown in Fig. 4, and is illustrative, as the droplet experiences hydrodynamic motion only. The measurement system correctly records a negligible temperature change during this measurement in Fig. 4, which is expected.

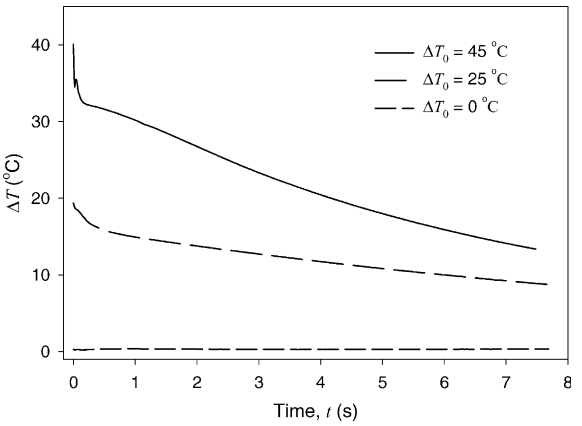

Fig. 4. Interface temperature difference for water droplet on the F2 prism.

The cases for $\Delta T_0 = 25$ and 45 °C exhibit an abrupt temperature increase as the droplet first strikes the prism at $t \approx 0$ s, followed by a cooling curve that decreases with time. Interestingly, for $\Delta T_0 = 45$ °C in Fig. 4 there is a small temperature fluctuation of ~2 °C roughly 40 ms after the liquid impinges upon the substrate. This is likely some artifact associated with the complex hydrodynamics of the droplet deformation and flow as it strikes the surface [2,3,6,7]. The temperature history in the first second of the two curves differs somewhat in shape, and may be due to slight variations in the droplet impingement site on the prism with respect to the laser interrogation region.

Also to note from the results is that the maximum temperature recorded from the technique is less than the temperature of the liquid, which is expected. In Fig. 4, for example, the maximum ΔT at the water–glass interface is ~18 °C for $\Delta T_0 = 25$ °C, and ~32 °C for $\Delta T_0 = 45$ °C. Heat flows from the hotter liquid to the solid at the interface upon contact, and thus the liquid near the interface is cooled by heat conduction into the glass substrate. Since the thermal penetration depth is much smaller than the size of both the droplet and substrate during the impingement process, the assumption of two semi-infinite bodies is applicable and the initial interface temperature rise can be given by [22,23]:

$$\Delta T_{\text{int}} = \frac{(\sqrt{k\rho C_p})_{\text{l}}}{(\sqrt{k\rho C_p})_{\text{l}} + (\sqrt{k\rho C_p})_{\text{g}}} \Delta T_0 \tag{10}$$

or, rearranging,

$$\frac{\Delta T_{\text{int}}}{\Delta T_0} = \frac{b_{\text{l}}}{b_{\text{l}} + b_{\text{g}}} \tag{11}$$

where b_{l} and b_{g} are the effusivities $(k\rho C_p)^{1/2}$ of liquid and glass, and ΔT_{int} is the interface temperature change. Referring to Table 1 for the thermal properties of water and F2 glass, Eq. (11) yields $\Delta T_{\text{int}}/\Delta T_0 = 0.56$, which corresponds to $\Delta T_{\text{int}} = 14$ °C for $\Delta T_0 = 25$ °C, and 25 °C for $\Delta T_0 = 45$ °C, which is slightly lower than the measured results for the first few hundred milliseconds in Fig. 4. A possible reason for this may be the internal flow and deformation of the droplet that brings hotter liquid from the top of the droplet towards the interface during impact, which is not accounted for in the simple conduction model above.

For the interface temperature measurement with glycerol, the experimental procedure is identical to that for water, and similar results are obtained as shown in Fig. 5, except for the case for $\Delta T_0 = 0$. Unusually large voltages fluctuations were observed just after the glycerol droplet strikes the dry substrate at $\Delta T_0 = 0$. The reason is that, due to its extremely high viscosity at room temperature, the impinging glycerol droplet does not remain in perfect contact with the substrate as it spreads quickly along the surface during impact, but rather entrains small air bubbles that are trapped at the interface. These air bubbles alter the reflectivity of the interface, resulting in significant fluctuations in the output voltage. These bubbles can also be observed visually by scattering of the laser beam in the droplet several seconds after the droplet comes to rest. Because of buoyancy, the bubbles at the interface will slowly move upward and the intensity of the reflected laser beam at the photodiode will decrease as the air bubbles are replaced by glycerol. It takes about 15 min for the bubbles to leave the interface and produce a gas-free contact at the liquid–glass interface. To test the stability of the system without the effect of bubbles, a compromise is made. First a droplet of glycerol is placed on the glass surface and allowed to rest for 30 min until all bubbles leave the surface. Then a second droplet at room temperature ($\Delta T_0 = 0$ °C) is allowed to fall onto the first, and the reflectivity signal observed. No significant signal change is recorded, as shown in Fig. 5.

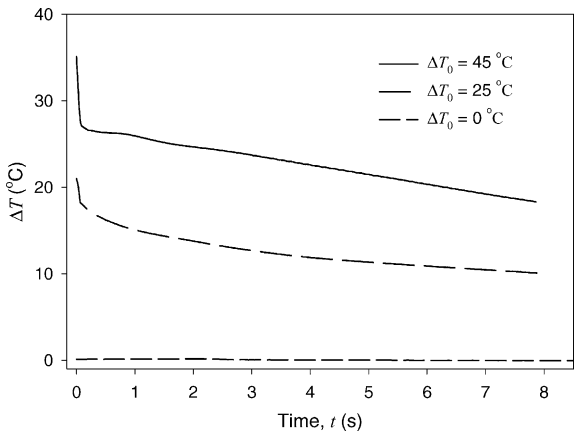

Fig. 5. Interface temperature difference for glycerol droplet on the F2 prism.

As glycerol is heated to higher temperature, e.g., $\Delta T_0 = 25$ and 45 °C, the viscosity and surface tension of glycerol are reduced dramatically, such that bubble entrainment is virtually eliminated. For glycerol at $\Delta T_0 = 25$ and 45 °C the results (Fig. 5) are similar to those for water, and also exhibit an abrupt temperature increase as the droplet first strikes the prism at $t = 0$ s, followed by a monotonically cooling curve. The recorded maximum interface temperature rises, ~18 °C for $\Delta T_0 = 25$ °C, and ~27 °C for $\Delta T_0 = 45$ °C, are also higher than the predicted initial interface temperature from the thermodynamic analysis in Eq. (11) for glycerol, i.e., $\Delta T_{\text{int}} = 11$ °C for $\Delta T_0 = 25$ °C, and 19 °C for $\Delta T_0 = 45$ °C.

4.2. Numerical model

A simple 1-D model is developed to compare with the experimental data. Although an analytical solution for this problem exists [24], it is based on infinite series and transcendental functions that must be evaluated numerically anyway. Also, flexibility in boundary conditions was desired. For these reasons, a simple numerical solution was adopted. When the droplet impinges on the horizontal prism surface, the droplet and prism are assumed to be in perfect thermal and physical contact. For 1-D heat conduction, the interface temperature and heat flux are then continuous at the interface [25]:

$$\left.\begin{aligned} T_{\text{l}} &= T_{\text{g}} \\ k_{\text{l}}\frac{\partial T_{\text{l}}}{\partial x} &= k_{\text{g}}\frac{\partial T_{\text{g}}}{\partial x} \end{aligned}\right\} \text{at the interface} \tag{12}$$

where T_{l} and T_{g} are the temperatures of the liquid and prism, and k_{l} and k_{g} are the thermal conductivities of liquid and prism, along the direction x normal to the interface, all respectively.

Such a model is applied to predict the interface temperature. Assuming 1-D heat conduction between two slabs placed in contact at time $t = 0$, the mathematic model in the rectangular coordinate system is (for $t \geqslant 0$):

$$\frac{\partial^2 T_{\text{i}}}{\partial x^2} = \frac{1}{\alpha_{T_{\text{i}}}}\frac{\partial T_{\text{i}}}{\partial t} \tag{13}$$

$$T_{\text{i}}(x, t = 0) = T_{\text{i0}} \tag{14}$$

$$\left(\frac{\partial T_1}{\partial x}\right)_{-L1} = \left(\frac{\partial T_2}{\partial x}\right)_{L2} = 0 \tag{15}$$

where T is temperature, x the direction normal to the interface, α_T the thermal diffusivity, and t time. Here $i = 1, 2$ represents the substrate and liquid, and T_{i0} and L_i are the initial temperature and thickness, respectively. The interface is located at $x = 0$, and the interface boundary conditions are represented by Eq. (12).

The 1-D conduction model above does not capture the complicated internal flow hydrodynamics, e.g. spreading and recoiling, associated with the droplet impingement, nor does it accurately capture the 2-D nature of heat conduction. For short times near the beginning of impingement, however, 1-D heat conduction dominates the interface temperature change, for the thermal penetration depth in this case is much smaller than the droplet diameter, and the heat transferred into the substrate is by conduction only. The model is solved using an implicit finite volume scheme with $L_1 = 0.5$ mm, $L_2 = 9.53$ mm, a uniform grid spacing $\Delta x = 10$ μm for both region 1 and 2, and a time step $\Delta t = 10$ μs.

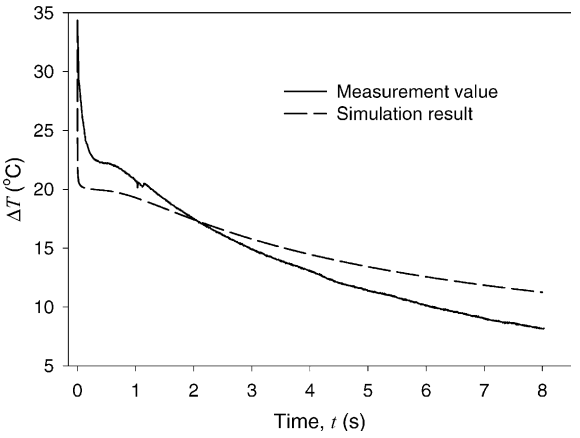

Fig. 6. Comparison of measurement and simulation for water on fused silica window for $\Delta T_0 = 35$ °C.

Both the measured interface temperature change and the simulation results for water on a 10 mm thick flat fused silica window with $\Delta T_0 = 35$ °C are shown in Fig. 6. (The modeling was done for earlier experimental results using a flat window and $\Delta T_0 = 35$ °C.) The trend is similar for $t \leqslant 0.4$ s, except that the measured interface temperature is somewhat higher than the simulation results. As discussed in the preceding part of this section, it may be due to the internal flow and deformation of the droplet during impingement. For times greater than 2–3 s, the measurement temperature drops more rapidly, which is attributed to 2-D conduction in the substrate.

5. Experiment uncertainty

The accuracy of both the liquid and glass refractive indices and their temperature coefficients significantly affects the measured temperature accuracy. Values of the refractive indices of F2 and glycerol and their temperature coefficients are reported in the literature with negligible uncertainties; however, the reported refractive index temperature coefficient for water, $\mathrm{d}n_{\text{l}}/\mathrm{d}T$, reported can vary by up to 14%. The measured temperature uncertainty associated with $\mathrm{d}n_{\text{l}}/\mathrm{d}T$ reaches a maximum when ΔT is a maximum, i.e., $\Delta T_0 = 45$ °C in this

work. The corresponding uncertainties are 6.3 °C for $\Delta T_0 = 45$ °C.

During the experiment, it is assumed that the measured photodiode voltage depends only on the interface temperature change; however, factors such as laser intensity drift, vibration of the optical components, noise in the photodiode and amplifier, and deviation in the beam incidence angle will also cause a voltage fluctuation in the measured signal. Among these factors, the largest contribution arises from the intensity drift in the HeNe laser, which is inherent in such lasers. A Coherent laser power analyzer was used to measure the laser intensity over a 3-min interval, and a drift of 0.1% was recorded. To quantify this variation, along with the others above, an isothermal interface was established using a water droplet at room temperature and measured over a 3-min period. The voltage fluctuation $\Delta V/V_0$ was ~0.31%, which corresponds to a temperature change of 0.5 °C. A more stable laser source, e.g., a thermoelectrically cooled laser diode, can reduce the laser fluctuations, and improve the measurement accuracy accordingly.

The uncertainty in the angle of incidence, α, also contributes to the measurement uncertainties. The mirror is mounted on a rotational stage with a scale uncertainty of $\pm 1/24°$. Accounting for the initial alignment of the stage to obtain a reference angle, the uncertainty in the incidence angle is taken to be $\pm 0.5°$, which corresponds to a temperature uncertainty of 0.1 °C. The extinction ratio of the linear polarizer is less than 10^{-5}; therefore, uncertainty due to any unpolarized light in the beam can be neglected. The HeNe laser output power is 5 mW, and the light intensity at the interface is ~2.0 mW. The linear absorption coefficient of water is on the order of 10^{-3} cm^{-1}, therefore liquid heating by the laser beam can be neglected.

Considering the above sources of the uncertainties, the computed root-sum-square uncertainty for the measured temperature for water is 6.3 °C for $\Delta T_0 = 45$ °C and 3.5 °C for $\Delta T_0 = 25$ °C. The main uncertainty source for water is the refractive index temperature coefficient, rather than the experimental configuration itself. If the uncertainty in the temperature coefficient is removed, the final measurement uncertainty is estimated to be 0.5 °C.

For glycerol, the bubbles formed at the glycerol–glass interface near room temperature are a source of error in addition to those discussed above, however, the effect of the bubbles are insignificant at higher temperatures, e.g., $T = 50$ °C.

6. Conclusions

This work presents a laser-based technique to measure the transient interface temperature for a liquid droplet impinging on a glass substrate. Thermoreflectance is used to monitor changes in the liquid and substrate refractive indices at the interface, from which the temperature variation is determined. The volume of the droplet is 40 μl, and initial temperature differences of 0, 25, and 45 °C have been tested, with a temporal resolution of 8.8 ms and a spatial resolution of 180 μm. The experimental setup is simple, inexpensive, and reliable, and is capable of measuring fast temperature changes with high temporal and spatial resolutions. Solidification and evaporation of droplet during impingement may also be possible to investigate with this technique with minor modification.

Acknowledgements

The authors gratefully acknowledge financial support for this work from the National Science Foundation through contract CTS–9702644.

References

[1] M. Rein, Phenomena of liquid-drop impact on solid and liquid surfaces, Fluid Dyn. Res. 12 (2) (1993) 61–93.
[2] C.D. Stow, M.G. Hadfield, An experimental investigation of fluid-flow resulting from the impact of a water drop with an unyielding dry surface, Proc. R. Soc. London, Ser. A—Math. Phys. Eng. Sci. 373 (1755) (1981) 419–441.
[3] W.M. Healy, J.G. Hartley, S.I. Abdelkhalik, Comparison between theoretical models and experimental data for the spreading of liquid droplets impacting a solid surface, Int. J. Heat Mass Transfer 39 (14) (1996) 3079–3082.
[4] S.T. Thoroddsen, J. Sakakibara, Evolution of the fingering pattern of an impacting drop, Phys. Fluids 10 (6) (1998) 1359–1374.
[5] J.P. Delplanque, R.H. Rangel, A comparison of models, numerical simulation, and experimental results in droplet deposition processes, Acta Mater. 46 (14) (1998) 4925–4933.
[6] N. Hatta, H. Fujimoto, H. Takuda, Deformation process of a water droplet impinging on a solid surface, J. Fluids Eng.—Trans. ASME 117 (3) (1995) 394–401.
[7] M.H. Shi, T.C. Bai, J. Yu, Dynamic behavior and heat-transfer of a liquid droplet impinging on a solid-surface, Exp. Therm. Fluid Sci. 6 (2) (1993) 202–207.
[8] A.F. Cokmeztuzla, K. Tuzla, J.C. Chen, Experimental assessment of liquid wall contacts in post-chf convective boiling, Nucl. Eng. Des. 139 (1) (1993) 97–103.
[9] T.Q. Qiu, C.P. Grigoropoulos, C.L. Tien, Novel technique for noncontact and microscale temperature measurements, Exp. Heat Transfer 6 (1993) 231–241.
[10] A.S. Lee, P.M. Norris, A new optical method for measuring surface temperature at large incident probe angles, Rev. Sci. Instrum. 68 (2) (1997) 1307–1311.

[11] C.H. Fan, J.P. Longtin, Laser-based measurement of liquid temperature or concentration at a solid–liquid interface, Exp. Therm. Fluid Sci. 23 (1–2) (2000) 1–9.
[12] T. Muller, G. Grunefeld, V. Beushausen, High-precision measurement of the temperature of methanol and ethanol droplets using spontaneous raman scattering, Appl. Phys. B—Lasers Opt. 70 (1) (2000) 155–158.
[13] Z. Zhao, D. Poulikakos, J. Fukai, Heat transfer and fluid dynamics during the collision of a liquid droplet on a substrate—II. Experiments, Int. J. Heat Mass Transfer 39 (13) (1996) 2791–2802.
[14] E. Hecht, Optics, second ed., Addison-Wesley, MA, 1987.
[15] F.A. Jenkins, H.I. White, Fundamentals of Optics, fourth ed., McGraw-Hill, New York, 1976.
[16] D. Solimini, Loss measurement of organic materials at 6328 a, J. Appl. Phys. 37 (8) (1966) 3314–3315.
[17] J. Stone, Measurements of the absorption of light in low-loss liquids, J. Opt. Soc. Am. 62 (3) (1972) 327–333.
[18] S. Kaschke, Schott 1996 Optical Glass Catalog, Schott Glaswerke, Mainz, Germany, 1996.
[19] D.R. Lide, D.R. Lide (Eds.), CRC Handbook of Chemistry and Physics, CRC Press, Boca Ration, FL, 1998.
[20] J. Timmermans, Physico-Chemical Constants of Pure Organic Compounds, Elsevier, New York, 1950.
[21] S.A. Self, Focusing of spherical gaussian beams, Appl. Opt. 22 (5) (1983) 658–661.
[22] H.S. Carslaw, J.C. Jaeger, second ed., Oxford University Press, London, UK, 1959.
[23] T. Loulou, D. Delaunay, The interface temperature of two suddenly contacting bodies, one of them undergoing phase change, Int. J. Heat Mass Transfer 40 (7) (1997) 1713–1716.
[24] F. De Monte, Transient heat conduction in one-dimensional composite slab. A 'natural' analytic approach, Int. J. Heat Mass Transfer 43 (19) (2000) 3607–3619.
[25] S. Kakac, Y. Yener, Heat Conduction, third ed., Taylor and Fancis, Washington, DC, 1993.